

ESTABLISHING A CONNECTION BETWEEN ACTIVE REGION OUTFLOWS AND THE SOLAR WIND: ABUNDANCE MEASUREMENTS WITH EIS/*HINODE*

DAVID H. BROOKS¹

College of Science, George Mason University, 4400 University Drive, Fairfax, VA 22030

HARRY P. WARREN

Space Science Division, Naval Research Laboratory, Washington, DC 20375

Draft version September 18, 2018

ABSTRACT

One of the most interesting discoveries from *Hinode* is the presence of persistent high temperature high speed outflows from the edges of active regions. EIS measurements indicate that the outflows reach velocities of 50 km s^{-1} with spectral line asymmetries approaching 200 km s^{-1} . It has been suggested that these outflows may lie on open field lines that connect to the heliosphere, and that they could potentially be a significant source of the slow speed solar wind. A direct link has been difficult to establish, however. We use EIS measurements of spectral line intensities that are sensitive to changes in the relative abundance of Si and S as a result of the first ionization potential (FIP) effect, to measure the chemical composition in the outflow regions of AR 10978 over a 5 day period in December 2007. We find that Si is always enhanced over S by a factor of 3–4. This is generally consistent with the enhancement factor of low FIP elements measured *in-situ* in the slow solar wind by non-spectroscopic methods. Plasma with a slow wind-like composition was therefore flowing from the edge of the active region for at least 5 days. Furthermore, on December 10–11, when the outflow from the western side was favorably oriented in the Earth direction, the Si/S ratio was found to match the value measured a few days later by ACE/SWICS. These results provide strong observational evidence for a direct connection between the solar wind, and the coronal plasma in the outflow regions.

Subject headings: Sun: corona—Sun: abundances—solar wind

1. INTRODUCTION

Recent observations by the EUV imaging spectrometer (EIS, Culhane et al. 2007) and X-ray telescope (XRT, Golub et al. 2007) on *Hinode* (Kosugi et al. 2007) have detected the presence of high temperature outflows at the edges of active regions (Sakao et al. 2007; Doschek et al. 2007; Harra et al. 2007). These outflows show velocities on the order of tens of km s^{-1} and the high spectral resolution EIS data have revealed that the line profiles have asymmetries that reach several hundred km s^{-1} (Bryans et al. 2010; Peter 2010). Similar outflows have been observed previously at lower temperatures as intensity perturbations in TRACE images (Schrijver et al. 1999), or Doppler shifts in SUMER spectra (Marsch et al. 2004), but the relationship between the cool and hot flows is only now being established through comprehensive studies using the broad temperature coverage of EIS (Del Zanna 2008; Warren et al. 2010). Active regions are thought to be possible sources of the slow solar wind, especially during solar maximum, and there have been several studies pursuing this connection (Neugebauer et al. 2002; Schrijver & De Rosa 2003; Liewer et al. 2004). It is important, however, to determine exactly where the slow speed wind is originating from in an active region. Wang et al. (2009) have stressed that the conditions at the base of open field lines greatly influence the properties of the wind in hydrody-

namic models. The persistence of the outflows for several days has led to the suggestion that they specifically could be the most significant contributors (Sakao et al. 2007; Harra et al. 2008; Doschek et al. 2008). A direct link has been difficult to establish, however, and further studies are needed, together with observational and theoretical investigations of the origin and driver of the outflows (Baker et al. 2009; Murray et al. 2010).

One capability of EIS that has not yet been fully exploited and could help in establishing a connection, is the ability to measure the chemical composition of the outflows. It is known from *in-situ* measurements of the ion composition in the slow speed solar wind that elements with a first ionization potential (FIP) below about 10 eV are enhanced by factors of 3–4 relative to their photospheric abundances (von Steiger et al. 2000; Feldman & Widing 2003). In contrast, the fast speed solar wind shows only a small enhancement; perhaps a factor of 1.5 (von Steiger et al. 2000), and this is also consistent with spectroscopic measurements in the coronal hole source regions that show abundances that are close to photospheric (Feldman & Laming 2000). For a discussion of explanations for the FIP effect see, e.g., Laming (2004). The magnitude of the FIP effect also appears to be related to the coronal plasma confinement time (Feldman & Widing 2003), so the source of the plasma that flows to the slow wind must be confined long enough to reach an enhancement factor of 3–4 and then must be released to the solar wind along open field lines.

Since the magnitude of the FIP effect varies substantially between different solar features

dhbrooks@ssd5.nrl.navy.mil

¹Present address: Hinode Team, ISAS/JAXA, 3-1-1 Yoshinodai, Sagamihara, Kanagawa 229-8510, Japan

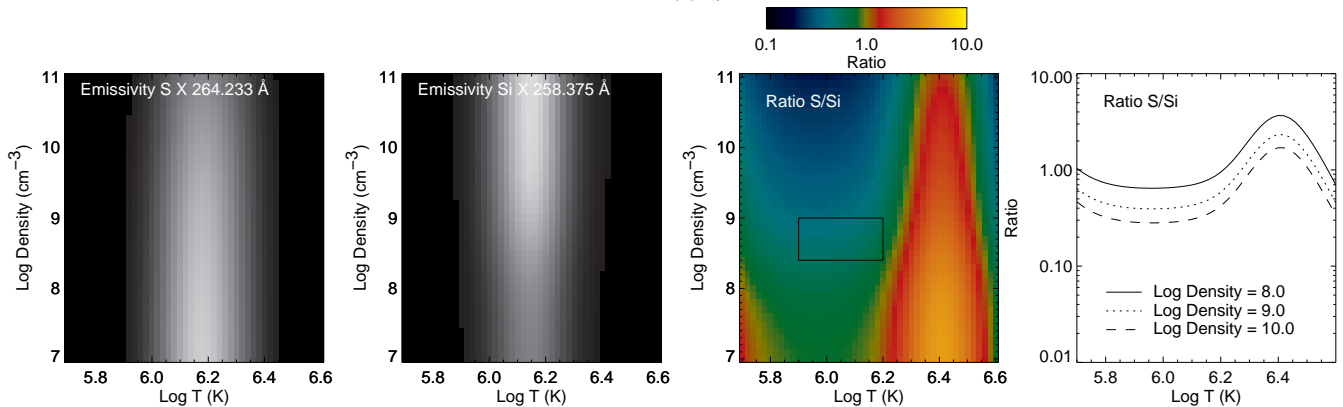


FIG. 1.— Si X 258.374 Å/S X 264.233 Å abundance diagnostic ratio. From left to right: emissivity as a function of temperature and density for S X 264.233 Å and Si X 258.374 Å. Ratio as a function of temperature and density and as a function of temperature for densities of $\log(N_e/\text{cm}^{-3}) = 8\text{--}10$. The boxed area indicates the $[T_e, N_e]$ space derived for the majority of the outflows.

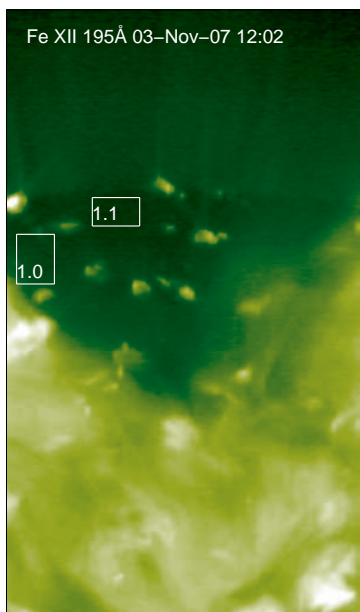


FIG. 2.— North polar coronal hole observation used as a test of the method for deriving the FIP bias. The derived values within the boxes are shown.

(Feldman & Widing 1993; Sheeley 1995, 1996; Raymond et al. 1997), the possibility exists that measurements of the magnitude of the FIP effect could identify the source location of the slow wind. Some previous work measuring the FIP-bias (ratio of coronal abundance of a low FIP element to that of a high FIP element) in the boundary between an active region and a coronal hole has been undertaken by Ko et al. (2006), who found that this could be a possible source location of the solar wind. Similar studies are rare, however, and to date there have been no measurements of relative abundances in the high speed outflows near active regions. Recently Feldman et al. (2009) outlined how EIS observations of Si and S lines could be used to measure the FIP bias at temperatures near 1.5 MK, the peak temperature for the active region outflows. They did not study the outflows, but gave a few illustrative calculations for a number of targets. They also noted that accurate measurements would require differential

emission measure (DEM) analysis. In this letter, we present the methodology needed to account for the temperature and density sensitivity of the emission lines involved and calibrate it with measurements in several polar coronal holes. We then measure the FIP-bias in the outflow regions of AR 10978 over a period of 5 days in December, 2007 and show that the results are consistent with the *in-situ* measurements.

2. DATA PROCESSING AND METHODOLOGY

The EIS instrument observes in two wavelength bands: 171–212 Å and 245–291 Å. It has 1'' spatial pixels and a spectral resolution of 22.3 mÅ. The instrument is described in detail by Culhane et al. (2007). In this letter, we analyze observations of AR 10978 obtained between December 10th and 15th, 2007. This region has previously been studied in detail by several authors (Doschek et al. 2008; Brooks et al. 2008; Warren et al. 2008; Ugarte-Urra et al. 2009; Bryans et al. 2010). The data we use were obtained with the 1'' slit in scanning mode. The observing sequence covers a large FOV of 460'' × 384'' with 40s exposures at each position and we use data from 5 runs of this sequence. Calibration and processing of the data were performed using standard procedures in SolarSoft. In addition, the orbital drift of the spectrum on the detector due to instrument thermal variations and spacecraft revolution were corrected using the artificial neural network model of Kamio et al. (2010). This model also corrects the spatial offsets between detectors and the spectral curvature caused by the grating tilt. It uses instrument temperature information and spacecraft housekeeping data to perform the correction, and the residual uncertainty of the wavelength positions is expected to be $\sim 4.5 \text{ km s}^{-1}$. The reference wavelength is taken from an average of all the mission data for the Fe XII 195.119 Å line, but we make an additional correction for Fe XIII 202.044 Å using the average value obtained in a relatively quiet area of the rasters. We use the lowest 50 pixels for this purpose.

The high spectral resolution of EIS enables observation of coronal emission line profiles in detail. In previous work we have found the line widths in the core of an active region to be narrow (Brooks & Warren 2009), however, several studies have identified blue-wing asymmetries associated with different solar features including

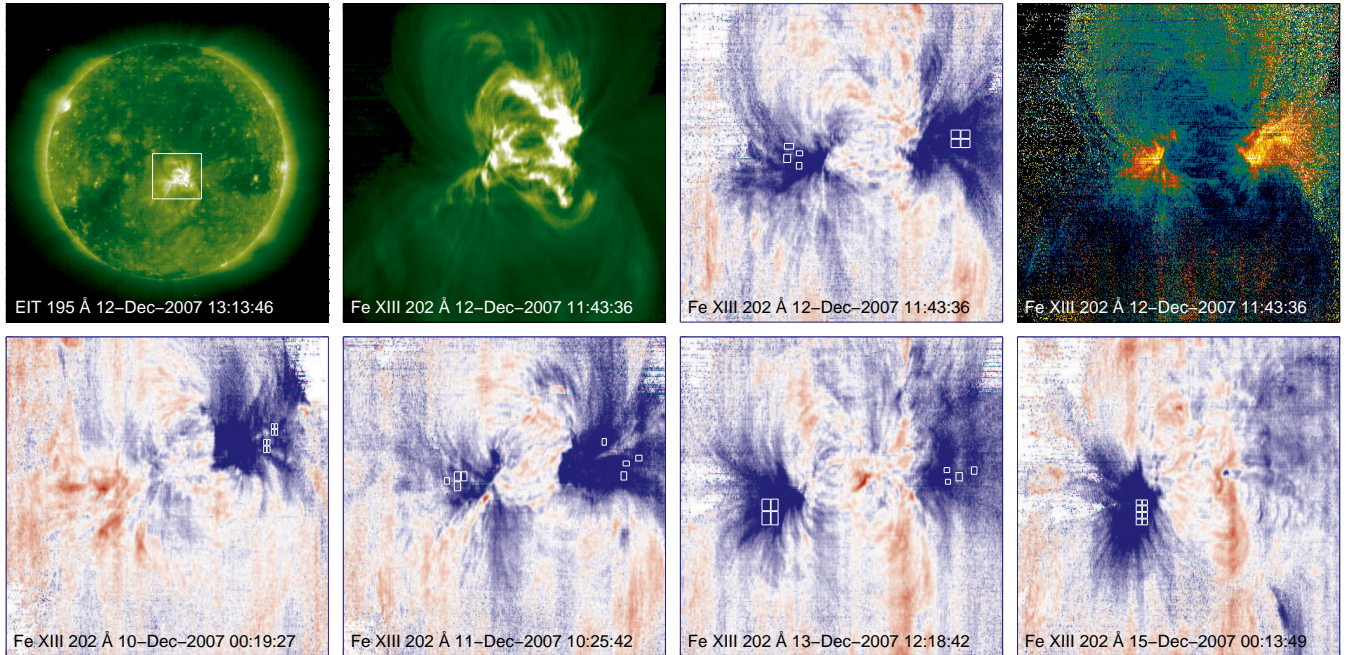


FIG. 3.— Context images and velocity maps for AR 10978. Top row: examples for December 12: EIT 195 Å filter image, EIS Fe XIII 202.044 Å intensity image, Fe XIII 202.044 Å Doppler velocity map, and Fe XIII 202.044 Å non-thermal velocity map. Bottom row: velocity maps for the other 4 days between December 10 and 15. The areas used for the analysis are shown by small boxes on the velocity maps.

the outflows (Hara et al. 2008; De Pontieu et al. 2009; Bryans et al. 2010; Peter 2010). A Gaussian function tends to broaden and shift towards the wings to account for this asymmetry, but here we mainly use the derived velocities to identify the outflow regions and are more concerned with the accuracy of the intensity measurements. Since the contribution of the asymmetry to the total line intensity is generally small, we fit the spectral features with single and multiple Gaussians.

A number of methods can be used to determine the FIP-bias (f_{FIP}) in the outflows and a detailed discussion of diagnostic ratios in the EIS wavelength range is given by Feldman et al. (2009). They show that the Si X 258.374 Å/S X 264.233 Å ratio is constant to within $\sim 30\%$ in the $\log(T_e/K) = 6.0$ to 6.2 range, which makes it useful for analysis of the outflows. We recomputed the ratio using the CHIANTI v6.0.1 database (Dere et al. 1997, 2009), and show it as a function of temperature and density in Figure 1. With these data we find that the ratio varies by $\sim 40\%$ in the $\log(T_e/K) = 5.7$ to 6.2 range, but deviates strongly at high temperatures. In regions with a significant high temperature emission measure then, the ratio should properly be convolved with the DEM distribution. We also find a significant sensitivity of the ratio to the electron density (factor of 2.3 between $\log(N_e/\text{cm}^{-3}) = 8$ and 10). So the density in the target region also needs to be measured and accounted for. As we will show below, the densities determined for the outflows do not vary sufficiently to cause a greater than 30% change in the ratio.

We adopt the following procedure for our analysis. First, we measure the density in the outflow region using the Fe XIII 202.044 Å/Fe XIII 203.826 Å diagnostic ratio. Then, we derive the DEM distribution using a series of Fe VIII–XVI lines to minimize uncertainties due

to elemental abundances. The specific lines used are: Fe VIII 185.213 Å, Fe IX 188.485 Å, Fe X 184.536 Å, Fe XI 188.216 Å, Fe XII 195.119 Å, Fe XIII 202.044 Å, Fe XIV 274.203 Å, Fe XV 284.160 Å, and Fe XVI 262.984 Å. The DEM is reconstructed using the Markov-Chain Monte Carlo (MCMC) algorithm distributed with the PINTOF-FALE spectroscopy package (Kashyap & Drake 1998, 2000). For all the calculations we adopted the photospheric abundances of Grevesse et al. (2007). The atomic data for this calculation were computed using the CHIANTI database at the fixed electron density previously measured for each outflow. Once the DEM is computed, the Si X 258.374 Å and S X 264.233 Å line intensities are calculated. Since Si and Fe are both low FIP elements, the calculated Si X 258.473 Å intensity should be well matched, but we scale the Fe DEM (if necessary) to make sure that it is. We find, however, that the difference is less than 20% for all the outflow regions we investigate. The ratio of the calculated to observed intensity for the high FIP S X 264.233 Å line is then the FIP bias, fully accounting for the temperature and density dependence of the emissivities.

As an independent check of the method we derived f_{FIP} values for eight polar coronal hole observations. Since the polar coronal hole is the presumed source of the fast speed solar wind, and the chemical composition there is close to photospheric, we should obtain values close to one if the method is working correctly. Figure 2 shows an example for observations taken on 2007, November 3. The EIS scan used the 2'' slit to cover an area of 300'' by 512'' in around 1 hour. The exposure time was 50s. The FIP bias was derived using spatially averaged line profiles from the indicated areas, and found to be 1.0 and 1.1, respectively. In all eight regions f_{FIP} was found to be $1.2 \pm 15\%$. This agreement with expect-

TABLE 1
 PROPERTIES OF AR 10978 OUTFLOWS MEASURED IN EIS SLIT SCANS.

Date	Start Time	Location	$v/\text{km s}^{-1}$	$\eta/\text{km s}^{-1}$	$\log(N_e/\text{cm}^{-3})$	$\log(T_p/\text{K})$	f_{FIP}
10-Dec-2007	00:19:27	West	-18.3	41.9	8.6	6.1	3.0
			-23.9	51.6	8.5	6.1	2.8
			-19.1	42.0	8.5	6.0	2.7
			-20.4	46.9	8.5	6.2	3.0
			-17.5	35.9	8.4	6.2	2.9
			-16.8	38.6	8.5	6.2	2.7
			-17.4	37.1	8.5	6.2	2.8
			-17.8	39.4	8.5	6.2	2.5
			-10.9	33.0	8.8	6.3	3.7
			-10.9	34.8	8.8	6.2	3.8
11-Dec-2007	10:25:42	East	-9.8	31.7	8.7	6.3	3.5
			-14.2	38.1	8.8	6.2	3.9
			-26.8	50.7	8.5	6.2	3.7
			-17.9	39.2	8.4	6.2	3.3
			-24.1	45.6	8.6	6.2	3.2
		West	-21.4	45.8	8.5	6.2	3.3
			-16.6	39.7	8.7	6.2	4.0
			-12.6	32.9	8.6	6.2	3.5
			-17.3	39.0	8.6	5.6	3.8
			-20.4	41.0	8.7	6.3	4.1
12-Dec-2007	11:43:36	East	-18.1	40.4	8.5	6.2	3.1
			-20.8	43.3	8.5	6.2	3.7
			-21.8	45.8	8.5	6.2	3.4
			-22.3	47.3	8.5	6.2	3.8
			-20.7	35.5	8.7	6.2	3.6
		West	-21.1	41.9	8.8	5.9	3.6
			-21.2	35.9	8.7	6.2	3.4
			-26.4	47.8	8.7	5.6	3.9
			-17.2	37.0	8.4	6.2	3.5
			-12.5	35.6	8.4	6.2	2.9
13-Dec-2007	12:18:42	East	-15.3	35.0	8.4	6.2	2.7
			-21.9	43.4	8.5	6.2	2.8
			-41.2	57.5	8.7	6.0	4.0
			-27.5	41.5	8.8	6.2	3.9
			-41.7	57.4	8.8	6.0	3.7
		West	-33.2	47.2	8.8	6.2	4.1
			-40.0	59.4	8.7	5.6	3.9
			-35.1	53.1	9.0	6.0	3.9
			-32.7	47.4	8.7	6.0	3.8
			-24.8	46.3	8.8	6.0	3.7

v - Doppler velocity.

η - non-thermal velocity.

N_e - electron density.

T_p - temperature of emission measure peak.

f_{FIP} - FIP bias.

tations gives us confidence that the method is working correctly.

3. RESULTS

Figure 3 shows context images of AR 10978 for December 12 when it was near disk center (top row). A *SOHO* Extreme ultraviolet Imaging Telescope (EIT, Delaboudiniere et al. 1995) full Sun image is shown with the EIS raster FOV overlaid as a box. Note that the preceding and following coronal holes are located outside of this FOV, so this region is a good target for examining the outflow regions in isolation from any interaction with the coronal hole boundaries where previous measurements of f_{FIP} have been made in other active regions (Ko et al. 2006). The figure also shows intensity, Doppler velocity, and non-thermal velocity maps all derived from Gaussian fits to the Fe XIII 202.044 Å line profile. The non-thermal velocity is computed by subtraction in quadrature of the thermal and instrumental widths. The thermal width is calculated assuming the peak temperature of each outflow (T_p in Table 1).

The on orbit instrumental width is assumed to be 56m Å (Brown et al. 2008).

One can generally associate the dark intensity areas at the east and west side of the active region with the blue-shifted emission and regions of large non-thermal velocity, though careful comparison would be needed to understand if they are related to each other in detail. Doppler velocity maps are also shown for December 10–15. These maps are used to select outflow regions for further analysis, and the chosen regions are shown by the small boxes. Since the S X line is weak in the outflows, averaging over a small area is necessary to increase the signal-to-noise ratio. We selected 40 locations in total in both the solar east and west outflow regions over the 5 days.

In making this selection, we only chose regions of outflow along the line-of-sight. For example, on December 10th, the solar east side of the AR presumably has an outflow, and this rotates into view on the 11th. On the 10th, however, this region shows only red-shifts and low non-thermal velocities, presumably due to line-of-sight

effects. On this day, we only chose areas in the blue-shifted west side outflow.

To ensure that our selected locations were really in the outflows, we measured the Doppler velocities. These and the non-thermal velocities are noted in Table 1. The results indicate that this AR shows bulk outflows of $9.8\text{--}41.7\text{ km s}^{-1}$ and non-thermal mass motions of $31.6\text{--}59.4\text{ km s}^{-1}$.

We then used the Fe XIII line ratio to measure the electron density and the results are also shown in Table 1. We find values in the range $\log(N_e/\text{cm}^{-3}) = 8.4\text{--}9.0$. These are broadly consistent with the results found by Doschek et al. (2008). The DEM distributions at fixed electron density were used to determine the peak temperatures of the outflows. The results are also shown in Table 1 and fall in the range $\log(T_e/\text{K}) = 5.6\text{--}6.3$. Finally, the calculated f_{FIP} measurements are also shown in Table 1 and fall in the range 2.5–4.1. This indicates that the FIP enhancement factors in the outflows are in agreement with expectations from the *in-situ* measurements in the slow wind.

4. SUMMARY

Using data from *Hinode* EIS we have studied the outflow regions of AR 10978 over 5 days in December 2007. We find that the outflows show Doppler velocities of -22 km s^{-1} and mass motions of 43 km s^{-1} on average. We also measured the electron density and temperature in the outflows and found average values of $\log(N_e/\text{cm}^{-3}) = 8.6$ and $\log(T_e/\text{K}) = 6.2$, respectively. Combining an emission measure analysis with the modeling of Si X and S X lines, we measured the FIP bias in the outflows of the active region away from any surrounding coronal holes. We found that Si is always enhanced over S by a factor of 2.5–4.1, with a mean value of 3.4. These results generally agree with the enhancement factors of low FIP elements measured *in-situ* in the slow solar wind by non-spectroscopic methods, and the enrichment was consistent throughout the observations. The fact that plasma with a similar composition to the slow speed wind was continuously flowing out from the edge of the active region for several days lends strong support to the suggestion that the outflows contribute to the slow wind. We therefore show new evidence of a direct connection between the slow speed solar wind, and the coronal plasma in the outflow regions.

To conclusively prove this connection, however, one

should directly compare the EIS Si /S ratio in the outflows with that measured in the slow wind three days later (the travel time to Earth). If the plasma flowing from the AR really reaches the slow wind at Earth, the *in-situ* measurements should match the spectroscopic ones. Daily averages of the Si /S ratio measured by the Solar Wind Ion Composition Spectrometer (SWICS, Gloeckler et al. 1998) aboard the Advanced Composition Explorer (ACE, Stone et al. 1998) are available for us to make this comparison for the disk passage of AR 10978. The EIS observations indicate that the western outflow was near central meridian and favorably oriented towards Earth on December 10–11. The best dates for the SWICS comparison are therefore December 13–14. We examined the SWICS Si /S measurements on these dates and found average values of 2.3 and 3.5, respectively. From Table 1 we see that for December 10–11 the EIS averages are 2.8 and 3.4, respectively. The EIS results are thus within 20% of the SWICS measurements. Note that no connection could be established before or after these dates, indicating that the influence of the outflows is only seen when they are near disk center. Further work will be needed to determine if AR 10978 is a rare case, and also to quantify whether the outflow contribution to the slow wind is dominant or not.

Finally, we note that there may be other areas of an active region which could contribute to the solar wind and larger more systematic studies are needed. We have made some preliminary measurements in several locations in the core of the December 2007 region and find the FIP bias to be similar to that of the outflows. It is difficult to see how these closed field regions could contribute *directly* to the solar wind since no blue-shifted Doppler signatures are seen there. They could, however, contribute indirectly, for example, by reconnecting with open field lines. At present the outflows are the only regions that are known to meet the two necessary conditions for direct contribution to the wind: upflow and composition.

We would like to thank Yuan Kuen-Ko for very helpful discussions. This work was performed under contract with the Naval Research Laboratory and was funded by the NASA *Hinode* program. *Hinode* is a Japanese mission developed and launched by ISAS/JAXA, with NAOJ as domestic partner and NASA and STFC (UK) as international partners. It is operated by these agencies in co-operation with ESA and NSC (Norway).

REFERENCES

- Baker, D., van Driel-Gesztelyi, L., Mandrini, C. H., Démoulin, P., & Murray, M. J. 2009, *ApJ*, 705, 926
 Brooks, D. H., Ugarte-Urra, I., & Warren, H. P. 2008, *ApJ*, 689, L77
 Brooks, D. H., & Warren, H. P. 2009, *ApJ*, 703, L10
 Brown, C. M., Feldman, U., Seely, J. F., Korendyke, C. M., & Hara, H. 2008, *ApJS*, 176, 511
 Bryans, P., Young, P. R., & Doschek, G. A. 2010, *ApJ*, 715, 1012
 Culhane, J. L., et al. 2007, *Sol. Phys.*, 243, 19
 De Pontieu, B., McIntosh, S. W., Hansteen, V. H., & Schrijver, C. J. 2009, *ApJ*, 701, L1
 Del Zanna, G. 2008, *A&A*, 481, L49
 Delaboudiniere, J.-P., et al. 1995, *Sol. Phys.*, 162, 291
 Dere, K. P., Landi, E., Mason, H. E., Monsignori Fossi, B. C., & Young, P. R. 1997, *A&AS*, 125, 149
 Dere, K. P., Landi, E., Young, P. R., Del Zanna, G., Landini, M., & Mason, H. E. 2009, *A&A*, 498, 915
 Doschek, G. A., et al. 2007, *ApJ*, 667, L109
 Doschek, G. A., Warren, H. P., Mariska, J. T., Muglach, K., Culhane, J. L., Hara, H., & Watanabe, T. 2008, *ApJ*, 686, 1362
 Feldman, U., & Laming, J. M. 2000, *Phys. Scr.*, 61, 222
 Feldman, U., Warren, H. P., Brown, C. M., & Doschek, G. A. 2009, *ApJ*, 695, 36
 Feldman, U., & Widing, K. G. 1993, *ApJ*, 414, 381
 Feldman, U., & Widing, K. G. 2003, *Space Science Reviews*, 107, 665
 Gloeckler, G., et al. 1998, *Space Sci. Rev.*, 86, 497
 Golub, L., et al. 2007, *Sol. Phys.*, 243, 63
 Grevesse, N., Asplund, M., & Sauval, A. J. 2007, *Space Sci. Rev.*, 130, 105
 Hara, H., Watanabe, T., Harra, L. K., Culhane, J. L., Young, P. R., Mariska, J. T., & Doschek, G. A. 2008, *ApJ*, 678, L67

- Harra, L. K., Hara, H., Imada, S., Young, P. R., Williams, D. R., Sterling, A. C., Korendyke, C., & Attrill, G. D. R. 2007, PASJ, 59, 801
- Harra, L. K., Sakao, T., Mandrini, C. H., Hara, H., Imada, S., Young, P. R., van Driel-Gesztelyi, L., & Baker, D. 2008, ApJ, 676, L147
- Kamio, S., Hara, H., Watanabe, T., Fredvik, T., & Hansteen, V. H. 2010, ArXiv e-prints
- Kashyap, V., & Drake, J. J. 1998, ApJ, 503, 450
- Kashyap, V., & Drake, J. J. 2000, Bulletin of the Astronomical Society of India, 28, 475
- Ko, Y., Raymond, J. C., Zurbuchen, T. H., Riley, P., Raines, J. M., & Strachan, L. 2006, ApJ, 646, 1275
- Kosugi, T., et al. 2007, Sol. Phys., 243, 3
- Laming, J. M. 2004, ApJ, 614, 1063
- Liewer, P. C., Neugebauer, M., & Zurbuchen, T. 2004, Sol. Phys., 223, 209
- Marsch, E., Wiegmann, T., & Xia, L. D. 2004, A&A, 428, 629
- Murray, M. J., Baker, D., van Driel-Gesztelyi, L., & Sun, J. 2010, Sol. Phys., 261, 253
- Neugebauer, M., Liewer, P. C., Smith, E. J., Skoug, R. M., & Zurbuchen, T. H. 2002, Journal of Geophysical Research (Space Physics), 107, 1488
- Peter, H. 2010, A&A, 521, A51
- Raymond, J. C., et al. 1997, Sol. Phys., 175, 645
- Sakao, T., et al. 2007, Science, 318, 1585
- Schrijver, C. J., & De Rosa, M. L. 2003, Sol. Phys., 212, 165
- Schrijver, C. J., et al. 1999, Sol. Phys., 187, 261
- Sheeley, N. R., Jr. 1995, ApJ, 440, 884
- Sheeley, N. R., Jr. 1996, ApJ, 469, 423
- Stone, E. C., Frandsen, A. M., Mewaldt, R. A., Christian, E. R., Margolies, D., Ormes, J. F., & Snow, F. 1998, Space Sci. Rev., 86, 1
- Ugarte-Urra, I., Warren, H. P., & Brooks, D. H. 2009, ApJ, 695, 642
- von Steiger, R., et al. 2000, J. Geophys. Res., 105, 27217
- Wang, Y., Ko, Y., & Grappin, R. 2009, ApJ, 691, 760
- Warren, H. P., Ugarte-Urra, I., Doschek, G. A., Brooks, D. H., & Williams, D. R. 2008, ApJ, 686, L131
- Warren, H. P., Ugarte-Urra, I., Young, P. R., & Stenborg, G.